Geomorphology xxx (xxxx) 108580

Contents lists available at ScienceDirect

Geomorphology

journal homepage: www.elsevier.com/locate/geomorph

Stream regularization index. A morphometric approach to quantify the longitudinal profile regularization stage

Francisco Abel Jiménez-Cantizano *, Loreto Antón

Dpto. de Ciencias Analíticas, Facultad de Ciencias, Universidad Nacional de Educación a Distancia (UNED), Senda del Rey 9, 20840 Madrid, Spain

ARTICLE INFO

Article history:
Received 3 September 2022
Received in revised form 5 December 2022
Accepted 30 December 2022

Keywords:
Streams
Regularization index
Morphometric analysis
Longitudinal profile
Stream regularization
Iberian Peninsula

ABSTRACT

Fluvial systems carve the Earth's surface under the influence of climate and tectonics. This process tends towards dynamic equilibrium conditions, in which rivers respond by regularizing their longitudinal profiles to a graded form. However, external forcings frequently interrupt this trend displacing the system to a transient state from which the system will evolve again with a tendency towards a graded form. In bedrock incising rivers, the longitudinal profile shape provides information on transient states, and quantifying the regularization level makes it possible to establish inferences about a river's evolutionary trend and its relationship with the influencing external forcings. This work presents a procedure for quantifying the regularization level of streams from the analysis of the shape of the longitudinal profiles. This procedure involves quantifying of the departure of the current shape of the longitudinal profile from that representing the graded long profile under dynamic equilibrium conditions. This comparison is quantified by two indices: 'stream regularization index_G', calculated for the entire long profile, and 'regularization index_g', calculated discretely along the long profile. To illustrate the usefulness of the indices and how they respond in different fluvial contexts and evolutionary stages, the longitudinal profiles of 14 streams from the central area of the Iberian Peninsula were analyzed. The results are interpreted together with the area-slope graph and the *Ksn* index, which corroborated the usefulness of this technique as a morphometric tool for quantifying the river maturity and identify tectonic regime transitions.

1. Introduction

Similar to other physical processes that take place under the influence of a force field working to reach an equilibrium, river erosion carves the Earth's surface (under the gravitational field), balancing bedrock uplift (Shaler, 1899; Morisawa, 1962; Flint, 1974; England and Molnar, 1990; Bishop, 2007). This process tends to move towards dynamic equilibrium conditions in which rivers respond by adjusting their rate of erosion. This can increase or decrease the part of the energy necessary for the transport of sediments, which act as an erosion tool (Demoulin et al., 2016). These processes can be recognized in the shape of the longitudinal (long) profile of a river, since this shape is precisely one of the observable and quantifiable results of the aforementioned balance (Gilbert, 1877; Davis, 1902; Mackin, 1948). As Willett and Brandon (2002) point out, a graded long profile implies that the fluvial erosion balances the relief generated by uplift, so that the topography does not change with time. A steady state, in this case, refers to a long-term condition in which the average incision rate balances the average rock uplift rate relative to the outlet (Whipple et al., 2013). Although the channel geometry can be highly variable depending on the forcing that perturbs landscapes (Whittaker et al., 2007), declining slopes along the length of the channel are related to the incision capacity; thus, it remains constant throughout the entire long profile in a concave asymptotic-upward geometry (Shaler, 1899; Hack, 1957; Morisawa, 1962; Flint, 1974; Mudd et al., 2018). There are a variety of mathematical formulations that can be used to describe the shape of the graded long profile of a river (Snow and Slingerland, 1987, and references therein). For example, Hack (1957) proposes a logarithmic expression that relates the elevation of each point of the longitudinal profile to the stream length. Thus, in a semi-log plot, the long graded profile should describe a straight line; the value of the mean bed particle size is assumed to be constant. Expanding this concept, Goldrick and Bishop (2007) propose a formulation of the equilibrium long profile form based on the relationship between the incision rate, the downstream discharge, and the effects of lithological variation. According to this formulation, the long profile equilibrium can be represented by a straight line in a logarithmic plot of the downstream distance versus the slope. Quadratic functions and three-parameter exponential models have also been proposed for describing the longitudinal profiles of aggrading, alluvial systems that are unaffected by significant lateral inputs of water or sediment under steady or quasi-steady conditions (Morris and Williams, 1997; Rice and Church, 2001). Furthermore, numerical methods make it possible to relate the shape of the long profile to the parameters that govern the incision process of a river through the so-called stream power incision

* Corresponding author.
E-mail address: fjimenez329@alumno.uned.es (F.A. Jiménez-Cantizano).

https://doi.org/10.1016/j.geomorph.2022.108580
0169-555/© 20XX

models (SPIMs) (Howard et al., 1994; Whipple and Tucker, 1999; Lague, 2014; Harel et al., 2016). These methods have been used for the study of both equilibrium conditions (e.g., Varrani et al., 2019; Wickert and Schildgen, 2019; Hergarten, 2020) and transitory situations far from equilibrium (e.g., Gasparini et al., 2006; Kwang and Parker, 2017; Sassolas-Serrayet et al., 2019).

From the adjustment of the mathematical expression that represents a theoretical longitudinal profile, different indices have been derived that make it possible to quantify the dependent relationships between the variables in this expression (e.g., Hack, 1975; Demoulin, 1998; Goldrick and Bishop, 2007; Vágó, 2010; Rodrigo-Comino and Senciales González, 2015). However, it is also possible to deduce the shape of a long profile that would theoretically correspond to the equilibrium condition through a reverse analysis. Any of these methodologies can be used to mathematically reconstruct that theoretical long profile with respect to certain boundary conditions, a critical drainage area, a threshold value and the outlet position (Tarboton et al., 1989; Montgomery and Foufoula-Georgiou, 1993; Sklar and Dietrich, 1998; Whipple and Tucker, 1999). A realistic result could not be achieved in all cases due to the limitations of the methods, which are mainly related to the difficulty of estimating variables that do not have a linear behavior (Roe et al., 2002; Lague, 2014; Kwang and Parker, 2017) and long profiles that are not fitted well by any particular mathematical form (Hovius, 2000). However, if due precautions to reduce the uncertainty are taken, and the most appropriate method is selected, the theoretical equilibrium long profile can represent a valuable reference that can be used to quantify the departures of the real long profiles from the steady state. In consequence, it allows one to make inferences about what the potential evolution of the incision is or should be, and even about the forcing that disturbs the incision.

In this paper, we present a new metric for the quantification of the differences between the longitudinal profile of a stream and the graded theoretical long profile that would be expected with the development of a constant gradient from the head to the outlet. Thus, the incision capacity will be homogeneous throughout the entire theoretical long profile (Sklar and Dietrich, 1998). This new metric makes it possible to quantify the differences in shape between the two longitudinal profiles, i.e., the real profile and the theoretical profile. The metric can be globally quantified to obtain a general view of the state of the river and discretely quantified along the long profile to identify differences in the regularization levels of different reaches. To illustrate the usefulness of this metric, we have analyzed the longitudinal profiles of 14 rivers that drain the reliefs of the Spanish Central System and the Iberian Range, both located in the central zone of the Iberian Peninsula. They are two contiguous reliefs with very different structures and geological histories, and thus they represent an ideal setting for verifying the results of the proposed analysis. For this same purpose, we have also calculated the *Ksn* index from channel slope-contributing drainage area scaling (Wobus et al., 2006; Whipple et al., 2013), and the records have been compared in terms of the identification of knickpoint types and the sectorization of long profiles.

2. Calculation of the indices

The procedure is based on the quantification of the morphological differences between the longitudinal profile of a river and the theoretical constant-gradient long profile, i.e., the graded long profile. The graded long profile is the long profile that the river would develop under dynamic equilibrium conditions, given the positions of its headwater and outlet. From among the multiple mathematical methodologies, we selected the stream-gradient index (*SL*) principle (Hack, 1973), which in principle seems to be the most suitable for bedrock rivers and has been widely used (e.g., Pérez-Peña et al., 2009; Troiani et al., 2014; Subiela Blanco et al., 2019; Piacentini et al., 2020; Viveen et al., 2021). First, the value of the total *SL* is calculated, given the present headwater and outlet positions for the studied stream (Fig. 1). To obtain the headwater position, we selected the highest point above which there is an accumulation area of 1 km^2, typically the value of the critical contributing area (Sklar and Dietrich, 1998; Whipple, 2004). *SL* is the slope value of the straight line that joins the headwater and the outlet of the longi-

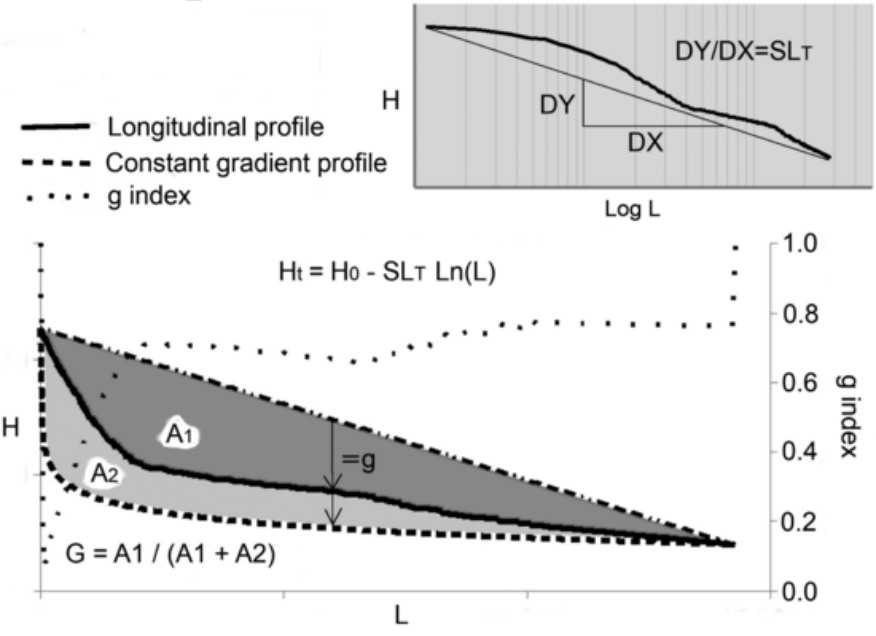

Fig. 1. Sketch of the methodology for the construction of the theoretical equilibrium longitudinal profile and the calculation procedure for the G and g indices. The upper plot illustrates the total stream-gradient index (SL_T) value, as the slope value of the straight line that joins the source and the outlet of the longitudinal profile plotted in a semilogarithmic graph. This value is required to obtain the elevation values of the theoretical long profile from the Hack equation. The lower plot illustrates a projected theoretical long profile (dashed line) together with a real long profile (solid line) and the procedure for obtaining the values of the indices. The G index value is the result of the areal difference between both profiles and the reference straight line that joins source and outlet. And g index is the sequence of discrete values (dots in the graph) resulting from the difference in elevation between the two profiles, measured with respect to the reference straight line that joins source and outlet. See the text for a detailed explanation.

tudinal profile plotted in a semilogarithmic graph (Fig. 1). The obtained *SL* value is then introduced into Hack's equation (Hack, 1973):

$$H_T = H_0 - SL \cdot \mathrm{Ln}(L), \quad (1)$$

where H_T is the constant-gradient long profile elevation, H_0 is the headwater elevation and L is the downstream distance measured from the headwater to the outlet. An elevation value (H_T) is obtained at each point along the constant-gradient longitudinal profile. The constant-gradient long profile is plotted against the present longitudinal profile (Fig. 1), and the morphological differences between these profiles are quantified using the straight line joining the headwater and the outlet as a reference. This line represents the available energy for stream erosion, to achieve the same erosive capacity along the entire profile, while the controlling variables on the system do not change. The quantification is made as follows: i) The difference in area between both longitudinal profiles with respect to the straight line joining the headwater and the outlet is calculated (Fig. 1). This returns a unique value for the entire long profile called stream regularization index_G. ii) The differences are measured in a discrete way, i.e., the elevation differences between both longitudinal profiles are measured at constant distance intervals. This metric provides a value called regularization index_g (Fig. 1). For the calculation of g, shorter distance intervals provide more complete information, although they also result in a higher computational cost.

2.1. Stream regularization index (G) interpretation

The G value provides quantitative information about the regularization level that a stream has reached in relation to its outlet. A G value equal to 1 means that the present long profile of the river matches the graded long profile. In this case, the river has reached its maximum incision level, given its current headwater and outlet elevations; it has already developed a constant-gradient long profile. Deviations from G equal to 1 happen when a stream is driving off the dynamic equilibrium conditions, and they are associated with a change in the gradient that does not correspond merely to a lithological contrast. Negative values of G are possible: they are associated with streams' long profiles under certain conditions, such as when they have a convex-up form. The results can also be read in terms of the percentage of the regularization level with respect to the maximum potential level; thus, a value of G equal to 1 represents 100 % of the maximum potential regularization, and all the intermediate terms down to 0 % can be interpreted in the same way.

2.2. Regularization index (g) interpretation

The discrete calculation makes it possible to assess the local regularization level and its spatial distribution along the stream. Hence, reaches with different regularization levels can be quantitatively identified. A value of 1 indicates the maximum regularization level at which the real long profile matches the theoretical constant-gradient longitudinal profile. A value of 0 occurs when the elevation of the present long profile at a given point coincides with the reference line, joining the headwater and the outlet (Fig. 1). This corresponds to a minimum regularization level with respect to the measurement reference. Negative values can occur in situations such as those mentioned above for G, for reaches that intersect the reference line. In fact, values >1 are possible, but they are usually limited to the lower reach. Values higher than 1 occur when the current long profile runs below the constant-gradient longitudinal profile. Otherwise, the trends of the g-value sequences offer valuable information on the fluvial changes. Three different general trend types are possible: i) Constant sequence of g values along a reach. This means that it is a constant-gradient reach since it follows a path parallel to the theoretical equilibrium long profile. This implies that the progressive slope decline, with all other factors considered equal, allows a homogeneous erosive capacity (Gilbert, 1877; Whipple et al., 2013). It is, therefore, a graded reach to a local base level or a preserved record from a previous evolution stage in which there was a different base level. If the value of g remains constant along the entire long profile, then the value of g will be 1, and we will have a fully graded long profile. ii) Downward trend of g values, which records a downstream loss of the gradient relative to the current outlet. It corresponds to a reach that moves away from the theoretical long profile in the downstream direction, indicating a loss in the erosive capacity. However, this can happen due to a purely geometric effect when the reach approaches the reference line that joins the headwater and the outlet of the stream, and this can occur even if the reach intercepts this line. In these cases, if the long profile shows a smooth concave geometry, analyzing just that reach of the long profile will result in a sequence of constant g values. iii) Upward trend of g values. This is always registered in sharp inflections. However, they also occur when the slope tends to be constant downstream, which results in an upstream decrease in the regularization level linked to a decrease in the gradient upstream. This is a typical shape for a long profile that moves towards more resistant materials requiring higher equilibrium slopes or an increase in the uplift ratio (Whipple and Tucker, 2002; Whittaker et al., 2007; Whittaker and Boulton, 2012).

The interpretation of the g-value sequences makes it possible to determine which inflections or changes in the longitudinal profile of a river are potentially due to a transition in the erosion rate, the lithology or a change in the base level due to different processes that influence landscape evolution. Typically, these changes are recorded in the form of knickpoints or knickzones, so that their identification, classification, and quantification (Whipple and Tucker, 1999; Wobus et al., 2006; Haviv et al., 2010; Kirby and Whipple, 2012; Whipple et al., 2013) make it possible to extract reliable information to solve the inverse problem of reconstructing the processes from the topography (e.g., Goldrick and Bishop, 2007; Whittaker and Boulton, 2012; Chauveau et al., 2021). For this purpose, automated algorithms have also been developed based on the statistical relationships of different variables that influence the shape of the longitudinal profile (e.g., Hayakawa and Oguchi, 2006; Gonga-Saholiariliva et al., 2011; Schwanghart and Scherler, 2014; Queiroz et al., 2015; Neely et al., 2017; Zahra et al., 2017; Gailleton et al., 2019); in this respect, the regularization index offers an alternative, simpler procedure. The g values always experience changes in the knickpoints, and these changes are variable depending on the type of knickpoint: there may be vertical-step knickpoints, slope-break knickpoints or knickzones (Haviv et al., 2010). Two sequences of constant g values separated by a sharp rise or a slightly decreasing sequence separated by a sharp rise from a sequence of downstream constant values correspond to a vertical-step knickpoint. Meanwhile, an ascending sequence of g values, preceded by a constant or decreasing sequence, is always associated with a slope-break knickpoint (Fig. 2).

The reason for this is that a vertical-step knickpoint always separates two sections of a river's long profile; these sections represent new and old equilibrium long profiles separated by the upstream propagating incision wave or a lithological contrast with a more erodible substrate downstream (Wobus et al., 2006; Whipple et al., 2013; Demoulin et al., 2016) so that, regardless of whether it is a mobile or anchored knickpoint, both reaches present a constant gradient. A constant gradient then implies a sequence of constant values of g because these values either fit the theoretical equilibrium long profile or follow a parallel path (Fig. 2). On the contrary, a slope-break knickpoint separates the longitudinal profile of a river into two reaches with different gradients; the gradient of the downstream reach is higher due to either an increase in the rock uplift rate or a lithological contrast that implies a more resistant substrate downstream (Wobus et al., 2006; Whipple et al., 2013; Demoulin et al., 2016). In this case, the values of g show an increasing trend downstream of the knickpoint as the long profile approaches the theoretical profile more and more and follows a trajectory that is nei-

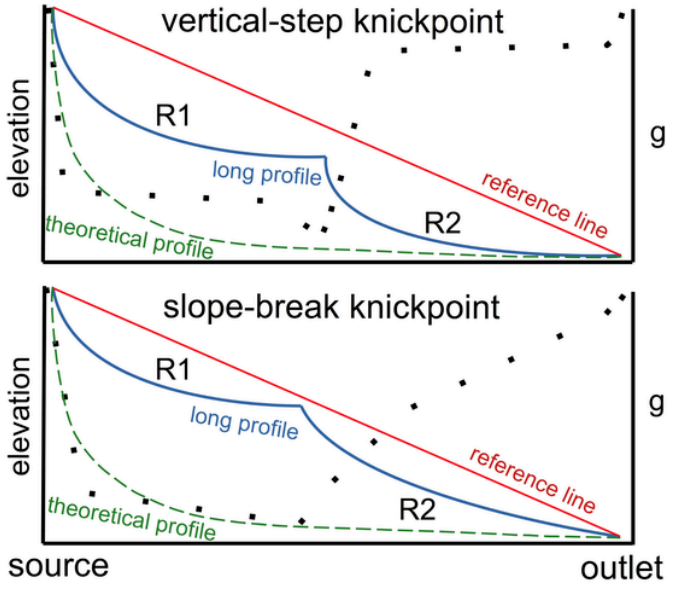

Fig. 2. Sketch showing two types of knickpoints in synthetic stream profiles (blue solid line) and their appearence on g values trend (dotted line). In a simplified way the upper plot shows two sequences of constant g values separated by a sharp rise, that correspond with two reaches, R1 and R2, separated by a vertical_step knickpoint. And the lower plot shows an ascending sequence of g values, preceded by a decreasing sequence, that correspond with two reaches, R1 and R2, separated by a slope_break knickpoint. (For interpretation of the references to colour in this figure legend, the reader is referred to the web version of this article.)

ther coincident nor parallel; the gradient, in this case, is always greater than the gradient of the calculated theoretical long profile (Fig. 2).

We can also consider two typical cases in which changes in the distribution of g values do not correspond to a significant change in the g-value trend. The first case corresponds to a knickzone, pointing to either disequilibrium in the downstream long profile or a steady-state spatial uplift gradient (Demoulin et al., 2016). The second case shows either small lithological contrasts (Chilton and Spotila, 2022) or the staggering derived from the limitations of the grid resolution when the long profile is obtained from a digital elevation model (DEM), as knic-knoise, for example (Hergarten, 2020).

3. Case study

3.1. Geological setting

We have analyzed the longitudinal profiles of the main rivers draining the eastern sector of the Spanish Central System reliefs (the Adaja, Cega, Duratón, Riaza, Alberche, Guadarrama, and Jarama rivers) and the central zone of the Iberian Range (the Jalón, Huerva, Aguas Vivas, Martín, Guadalope, Tajuña, and Guadiela rivers), which are located in the central area of the Iberian Peninsula (Fig. 3). These areas have two very different geological contexts, but they are annexes in the same geographical position, and therefore they have similar climatic histories (Pérez-Obiol et al., 2011; Oliva et al., 2019). The Spanish Central System extends for about 700 km in the NE-SW direction; with an average width of about 60 km and a maximum elevation of 2592 m asl. It is a large thick-skinned, double vergence crustal pop-up consisting of igneous rocks (mainly granites) and metamorphic rocks deformed by NE-SW to E-W thrusts that result from crustal uplift related to lithospheric folding. However, the main tectonic transport is southward directed, whereas in the north, the tectonic structure appears as a series of imbricate thrusts with smaller individual displacements (De Vicente et al., 2018 and references therein). The easternmost sector of the Spanish Central System lies within the Iberian Range, a mountain chain that extends for about 460 km in the NW–SE direction with an average width of about 90 km and a maximum elevation of 2315 m asl. It is a fold-and-thrust belt developed during the late Eocene to Miocene because of the contractional inversion of a series of Mesozoic rift basins, resulting from the convergence between the Eurasian, Iberian and African plates (Guimerá et al., 2004; Guimerá, 2018; Rat et al., 2019). The result is a NW-SE oriented doubly vergent intraplate mountain belt consisting of sedimentary rocks (mainly limestones), which boundaries with its surrounding foreland basins are always thrusts (Guimerá, 2018). The thrust-sheet on top of the edge thrusts, display two anticlinoriums, separated by a big synclinorium. They are interpreted as major fault-bend folds developed over the ramp and flat geometry of two major thrusts (Guimerá, 2018; Guimerá, 2022). The major part of the Iberian Chain is thick-skinned, as it involves together the Variscan basement and the Mesozoic and Cenozoic cover. Only the more external parts are thin-

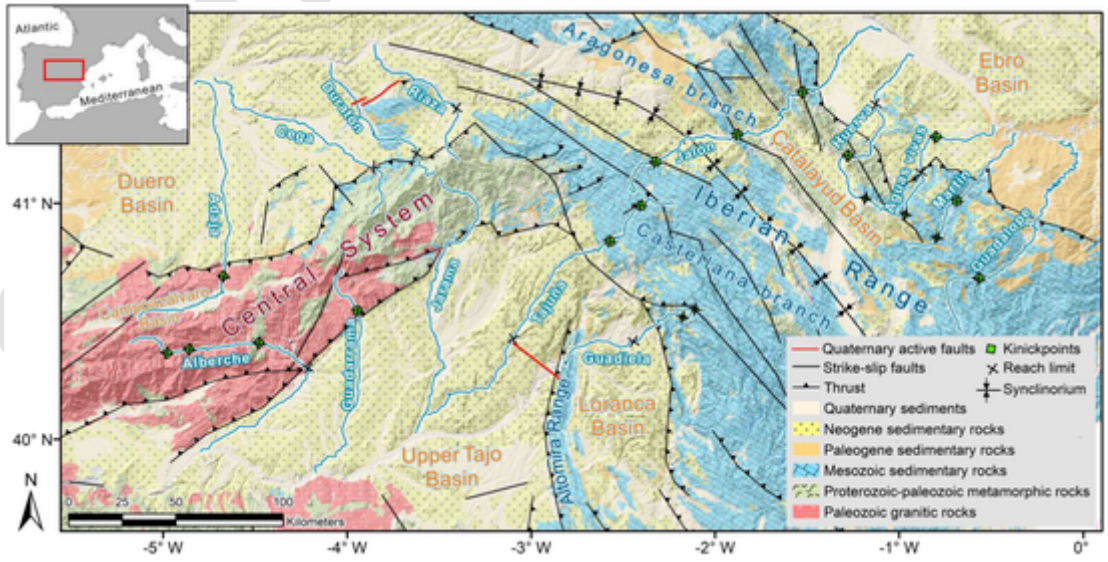

Fig. 3. Sketch of the geological context of the studied rivers. The delineation of the different lithological units is based on the IGME geological map of the Iberian Peninsula and the Balearic and Canary islands (Caride de Liñán, 1994). The locations of tectonic structures are based on the QAFI v.2.0 mapping of active Quaternary faults (García-Mayordomo et al., 2012). The limits of the reaches and the knickpoints that coincide with these limits on the river are included.

skinned. Its relief has a strong areal coincidence with all this contractional structures and they are genetically related. Highlights planation surfaces developed onto the orogenic building, overlain by the alluvial systems directed to, currently inverted, endorheic basins (Guimerá, 2018). The central sector of the Iberian Range outcrops in two parallel alignments, the Aragonesa branch to the east and the Castellana branch to the west, which are separated by the so-called Catalayud Basin. The Loranca piggy-back basin stands out on the western edge, and its thrust front is located in the Sierra de Altomira (Guimerá, 2018) (Fig. 3).

The link between the Spanish Central System and the Iberian Range occurs through a transpressive shear zone, which puts the outcrops of metamorphic rocks of the former in contact with the limestone outcrops of the latter. It is <10 km long, and is associated with the thrusting of the basement. In this transition zone between the Iberian Range and the Central System, both reliefs present a similar staggered folding structure in the NE–SW direction; (De Vicente et al., 2007). In both described reliefs, a marked lithological contrast occurs at their bounds, which correspond to the limits of the mountainous front next to the adjoining sedimentary basins, i.e., the Tajo, Ebro, and Duero basins (Fig. 3). All three of these basins are large Cenozoic intracratonic basins that are mainly filled with siliciclastic sediments at the margins and evaporites in central areas. This occurred under an endorheic regime initially, and then the basins were inverted, conceivably at different times. However, the mechanism responsible for the opening of the closed basins is still a topic of debate (Martín-Serrano, 1991; Santisteban et al., 1996; Pereira et al., 2000; Antón et al., 2012; Garcia-Castellanos and Larrasoaña, 2015; Antón et al., 2019; Cunha et al., 2019; Struth et al., 2019; Karampaglidis et al., 2020; Rodríguez-Rodríguez et al., 2020; Regard et al., 2021). Endorheic–exorheic transitions imply major geodynamic changes, which notably influenced the reorganization of drainage networks (Bridgland et al., 2020). One of the responses of the rivers to this process has been the readjustment of their longitudinal profiles to the new exorheic base level. However, each river system has responded differently to local and regional conditions, such as periglacial processes in high mountain headwaters, glacio-eustatic sea-level changes, and different tectonic patterns (Santisteban and Schulte, 2007).

3.2. Construction of the longitudinal profiles

The information required to construct the longitudinal profiles of the studied streams was extracted from the 90-m-cell-size digital elevation model SRTMv.4.1 (Jarvis et al., 2008) using the FLUNETS tool (Pastor-Martín et al., 2018). By using a sampling range of about $\delta\sqrt{2}$ (where δ is the grid resolution) along the vectorized streams, the elevation (H), and contributing area (A) data were obtained.

3.3. S_A plot and Ksn calculation

The *S-A* plot has been created, and the corresponding *Ksn* index calculation (Wobus et al., 2006) has been carried out in order to establish a comparison with the g values, especially with regard to the interpretation of the g-value trends. Stream power-law scaling or Flint's law, sets a continuous negative slope alignment that adjusts to a potential distribution under steady state or dynamic equilibrium conditions (Morisawa, 1962; Hack, 1973; Flint, 1974; Howard et al., 1994; Harel et al., 2016; Hergarten, 2020):

$$S = ksA^{-\theta}, \tag{2}$$

where S is the local channel slope, ks is the channel steepness index, A is the upstream drainage area, and θ is the concavity index. This function is only valid for drainage areas above a critical threshold, Acr, variably interpreted as the transition from divergent to convergent topography or from debris-flow to fluvial processes (Montgomery and Foufoula-Georgiou, 1993; Sklar and Dietrich, 1998; Whipple and Tucker, 1999; Wobus et al., 2006; Kirby and Whipple, 2012). *S-A* plot support the steady state assumption, and from the best fit linear regression can be inferred concavity and steepness indices value. On the other hand, the breaks in this scaling may be associated with records of transient conditions (Wobus et al., 2006; Kirby and Whipple, 2012; Whipple et al., 2013;). For example, knickpoints may separate segments with both similar or distinct steepness and concavity indices, depending on the spatial distribution of substrate properties, variations in rock uplift rates, and/or climatic factors (Whipple, 2004; Whipple et al., 2013; Demoulin et al., 2016). To identify distinct channel segments and the appropriate regression limits for each segment in *S-A* plot, the method proposed by Wobus et al. (2006) uses a reference concavity index (θ ref.) for the normalized steepness index (*Ksn*) determination, which allows the comparison of the steepness of channels in different drainage areas:

$$Ksn = KsA_{cent}^{(\theta\ ref-\theta)}, \tag{3}$$

and

$$A_{cent} = 10^{(\mathrm{Log}Amax+\mathrm{Log}\ Amin)/2}, \tag{4}$$

where Ks and θ are determined by regression, A_{max} and A_{min} bound the segment of the profile analyzed, and A_{cent} is the midpoint value for the segment analyzed (Wobus et al., 2006).

The slopes' values can be influenced by the uncertainty that causes noise in their distribution, which is related to the data collection itself and the precision of the DEM (Eckert et al., 2005; Wobus et al., 2006; Jarvis et al., 2008; Boulton and Stokes, 2018), and by the natural heterogeneities of the rocky beds that sometimes show a steepness associated with fractures and not related to the regional erosion rate (Mudd et al., 2018). For these reasons, an exponential smoothing of the data has been carried out with a constant or weighting factor of 0.1. This involves an application of the weighted moving average in which exponentially smaller weights are assigned as the slope decreases. A low value of the weighting factor was assigned because the greatest uncertainty occurs at the lowest values of S.

The value of θ ref., or m/n, in the *Ksn* calculation (Wobus et al., 2006) is usually taken as the regional mean of observed θ values in an undisturbed channel segment. Whipple and Tucker (1999) suggested that θ should fall in the range $0.35 \leq \theta$ ref. ≤ 0.6 if bedrock incision is driven by shear stress, so it is frequently assumed to be equal to 0.5, with n assumed to be 1. However, recent compilations of data from multiple landscapes show that this may not be the case (e.g., Lague, 2014; Clubb et al., 2016; Harel et al., 2016), and numerical modeling studies show that, in some specific situations, 0.5 leads to unrealistic relief structures (Kwang and Parker, 2017). Perron and Royden (2013) propose, for the determination of θ ref., the value that allows the best regression fit for the linearization of river longitudinal profiles or the chi integral approach. Additionally, Mudd et al. (2018) demonstrate that the integral method is the best method for calculating the most likely θ ref. for the analysis of rivers of the same network. In this study, we compare the longitudinal profiles of rivers from different catchments. Thus, for the estimation of θ, we have adopted the value of the best statistic according to average least-squares regression instead of the maximum likelihood estimator from chi-integral methods. The value obtained is 0.45 (Fig. 4).

4. Results

The longitudinal profiles of the rivers that drain the northern edge of the Spanish Central System have a smooth concave-up geometry. The G values range between 0.64 and 0.88, with an average value of 0.81 (Table 1). High values of g, which range between 0.5 and 1, have been obtained, except for at the headwaters, where the initial values drop to 0.1. In the case of the Adaja River, these values highlight a large inflec-

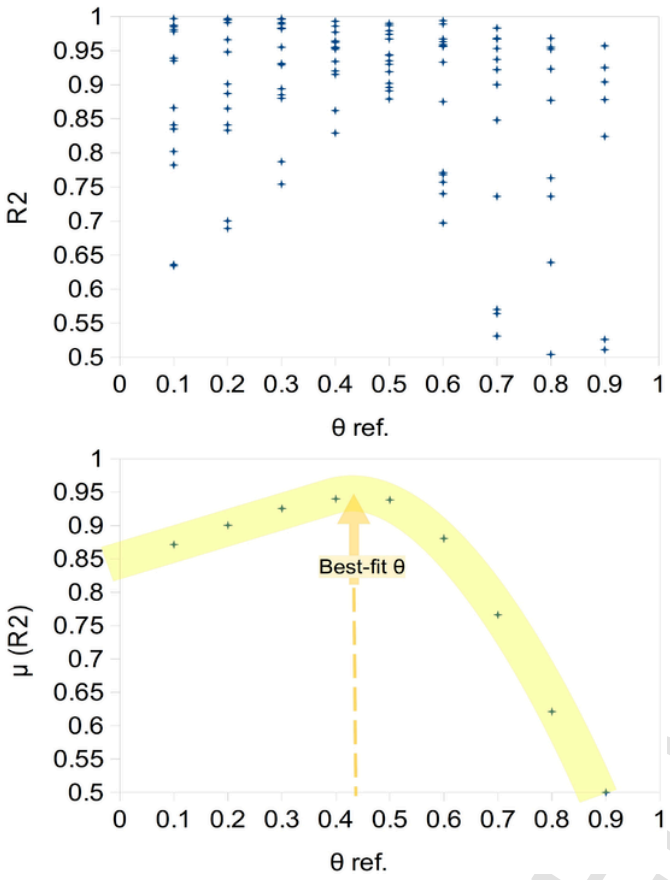

Fig. 4. Sketch showing the data plot from the best regression fit for the linearization of river longitudinal profiles and the determination of best statistic according to average least-squares regression, which was assumed to be the most likely θ ref.

tion or knickpoint, which divides this river into two halves. Using the g-value trend, two reaches, R1 and R2, have been differentiated in each long profile, except for that of the Adaja River, which has three reaches, R1, R2, and R3. These reaches have been identified in the S-A plot, and the corresponding *Ksn* values decrease downstream in a range from 156 to 21 (Fig. 5 and Table 1).

The longitudinal profiles of the rivers that drain the southern edge of the Spanish Central System have a more complex geometry. The longitudinal profile of the Alberche River has three great knickpoints joining reaches in a concave-up geometry. The Guadarrama River has a great knickpoint, and the Jarama River's profile is softer, with less concavity (Fig. 6). The G values range between 0.66 and 0.57, with an average value of 0.61 (Table 1). The obtained g values cover the entire possible range, although it is interesting that in three cases, they range from approximately 0.1 to 0.6 for the middle-upper half of the long profile, and values >0.6 are found for the middle-lower half. Using the g-value trends, five reaches have been differentiated for the Alberche River, two have been differentiated for the Guadarrama River, and only one has been distinguished for the Jarama River. These reaches have been identified in the S-A plot, and the corresponding *Ksn* values range from 95 to 23 (Fig. 6 and Table 1).

The longitudinal profiles of the rivers that drain the western edge of the Iberian Range have two different shapes. The long profile of the Tajuña River is low concavity, slightly staggered and fairly constantly steep. On the contrary, the Guadiela River presents a long profile with marked knickpoints in the upper-middle section, a softer concave-up shape in its lower-middle section, and a sharp drop to the end of the profile. G values of 0.24 and 0.55 have been obtained for the Tajuña and Guadiela rivers, respectively (Table 1). The obtained g values range between 0.1 and 0.4 for the long profile of the Tajuña River, and they range between 0.1 and 0.6 for the Guadiela River. Using the g-value trends, four reaches have been differentiated for both rivers. These reaches have been identified in the *S-A* plot, and the corresponding *Ksn* values range from 114 to 27 (Fig. 7 and Table 1).

The longitudinal profiles of the rivers that drain the eastern edge of the Iberian Range generally have a low concavity shape, except that of the Guadalope River, which follows a markedly downward slope. All of these profiles have numerous inflections. The G values range between 0.14 and 0.58, with an average value of 0.32 (Table 1). The g values have been obtained from the entire range; however, in the case of the Huerva and Aguas rivers, most of the g values do not exceed 0.4. Using the g-value trends, four reaches have been differentiated for the Jalón, Huerva, and Aguas rivers, three reaches have been identified for the Martín River, and two reaches have been identified for the Guadalope River. These reaches have been identified in the *S-A* plot, and the corresponding *Ksn* values range from 97 to 23 (Fig. 8 and Table 1).

5. Discussion

The G results allow us to see a clear difference between the rivers of the two mountain systems chosen as examples. The Spanish Central System has an average G value of 0.72 ± 0.13, while the Iberian Range has an average G value of 0.34 ± 0.16 (Table 1). This implies that the longitudinal profiles of the rivers that drain the Spanish Central System are graded approximately 70 %, while those of the Iberian Range only 30 %. The G values also show a significant difference between the average regularization levels of the rivers that drain the northern and south-

Table 1
Values of the Stream regularization index (G) of the longitudinal profiles of the example rivers. Mean G values and standard deviation are calculated for each mountain range and flanks. Values of *Ksn* are calculated for the delimited reaches in the longitudinal profiles of each river (Figs. 5 to 8).

Range		Catchment	River	G	Average (G)		Standard deviation (G)		*Ksn* ($m^{0.9}$)				
Spanish Central System	North	Duero	Adaja	0.64	0.81	0.72	0.11	0.13	38	33	31		
			Cega	0.87					122	21			
			Duratón	0.88					156	37			
			Riaza	0.83					127	31			
	South	Tajo	Alberche	0.57	0.61		0.04		59	80	95	78	23
			Guadarrama	0.6					42	38			
			Jarama	0.66					66				
Iberian Range	West		Tajuña	0.24	0.40	0.34	0.22	0,16	34	35	42	45	
			Guadiela	0.55					113	114	91	27	
	East	Ebro	Jalón	0.34	0.32		0.16		25	49	70	87	
			Huerva	0.24					33	27	42	59	
			Aguas Vivas	0.32					29	54	62	97	
			Martín	0.14					23	65	95		
			Guadalope	0.58					59	67			

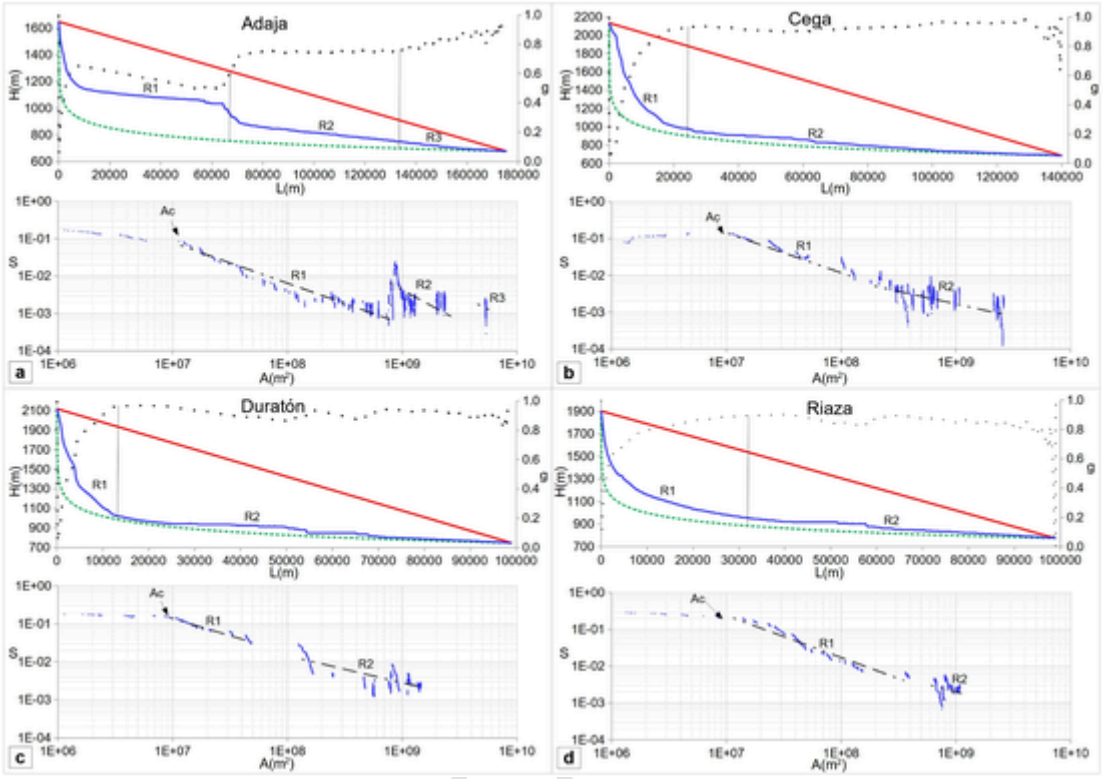

Fig. 5. Streams draining the northern flank reliefs of the Spanish Central System. The solid blue line represents the longitudinal profiles plotted together with the theoretical longitudinal profile (green dashed line) of each river. The g values are shown as a sequence of points. The straight red line is the reference with respect to which the indices have been calculated. The different identified reaches are shown for each long profile, along with the corresponding slope-area plots (log *S* vs. log *A*). *Ac* marks the transition to fluvial scaling. It highlights the elevation coincidence of the head reach limit. A third reach (R3) is distinguished only in the long profile of the Adaja River. See the text for a detailed interpretation. (For interpretation of the references to colour in this figure legend, the reader is referred to the web version of this article.)

ern flanks of the Spanish Central System, which are about 80 % and 60 %, respectively. Between the two flanks of the Iberian Range, this difference is smaller (around 10 %). On the other hand, if we compare the results for different drainage basins, we obtain more apparent differences in the average G values. Hence, an average level of regularization of about 30 % is obtained for the rivers that drain into the Ebro Basin, a level of regularization of about 50 % is obtained for those that drain into the Tajo Basin, and a level of regularization of about 80 % is obtained for those that drain into the Duero Basin. Since the drainage networks in the Spanish Central System reliefs incise more resistant rocks, i.e., granitic and metamorphic rocks, compared to the sedimentary carbonate rocks of the Iberian Range (Fig. 3), the described differences suggest a relationship with the differential Plio-Quaternary tectonic evolution of the Iberian Range with respect to its surroundings (Soria-Jáuregui et al., 2019; Struth et al., 2019; Galve et al., 2020). Uplift rates between 0.25 and 0.55 mm/y for the Iberian Cordillera (Giachetta et al., 2015; Conway-Jones et al., 2019) and about 0.1 mm/y for the Central System (Conway-Jones et al., 2019) haven been estimated. However, the differences in G values observed between the two flanks of the Spanish Central System (Table 1), may be best explained in relation with the structural asymmetry that this mountain range presents (Tejero et al., 2006; De Vicente et al., 2018). In addition, a post-inversion diachronic reorganization of the respective drainage networks happened (Garcia-Castellanos and Larrasoaña, 2015; Cunha et al., 2019; Karampaglidis et al., 2020; Rodríguez-Rodríguez et al., 2020; Regard et al., 2021; Benito-Calvo et al., 2022), which would explain the differences also found between the profiles of the rivers of each flank of each mountain range.

Beyond the general regularization levels of rivers, the g values provide a more detailed record. From the outset, the g metric is also clearly different between the rivers of the two mountain ranges, both in terms of values and values distribution. The longitudinal profiles of the rivers from the Spanish Central System have high values in quite a homogeneous distribution so that in most of them, only two different reaches are identified (Figs. 5 and 6). On the contrary, for the longitudinal profiles of the rivers from the Iberian Range, the values are generally low and have a heterogeneous distribution; in most of these profiles, four different reaches are identified (Figs. 7 and 8). The changes in the g-value trends highlight tectonic signals. The increasing sequences of g values show an erosive deficit upstream in the longitudinal profiles of the rivers of the Iberian Range (Figs. 7 and 8). It occurs downstream of the knickpoints, which suggests that they are slope-break knickpoints. In a systematic way, the first identified reach, R1, ends in these longitudinal profiles between elevations of 1000 and 1100 m asl. This elevation coincidence makes it possible to identify a temporary change in the rate of tectonic uplift, which causes a propagation at a constant rate of these slope-break knickpoints (Wobus et al., 2006; Whipple et al., 2013). There is not an elevation coincidence for the other succeeding knickpoints, which do coincide with changes in the g-value trend (Figs. 7 and 8). Nevertheless, they are related to tectonic structures. They stand out in the central zone of the Iberian Range in relation to a significant concentration of active Quaternary faults (García-Mayordomo et al., 2012; Sanz de Galdeano et al., 2020) (Fig. 3). The typology of the knickpoints and their relationship with active tectonics are verified using the S-A plot and *Ksn* values. Figs. 6 and 7 show descending data alignments linked by sharp rises, coinciding with the knickpoint locations, which are typical records of slope-break knickpoints (Wobus et al., 2006; Whipple et al., 2013). This is confirmed by the rising *Ksn* values downstream (Goren et al., 2014), as we can see in Table 1. In the case of the Jalón River (Fig. 8), the record of the knickpoints is some-

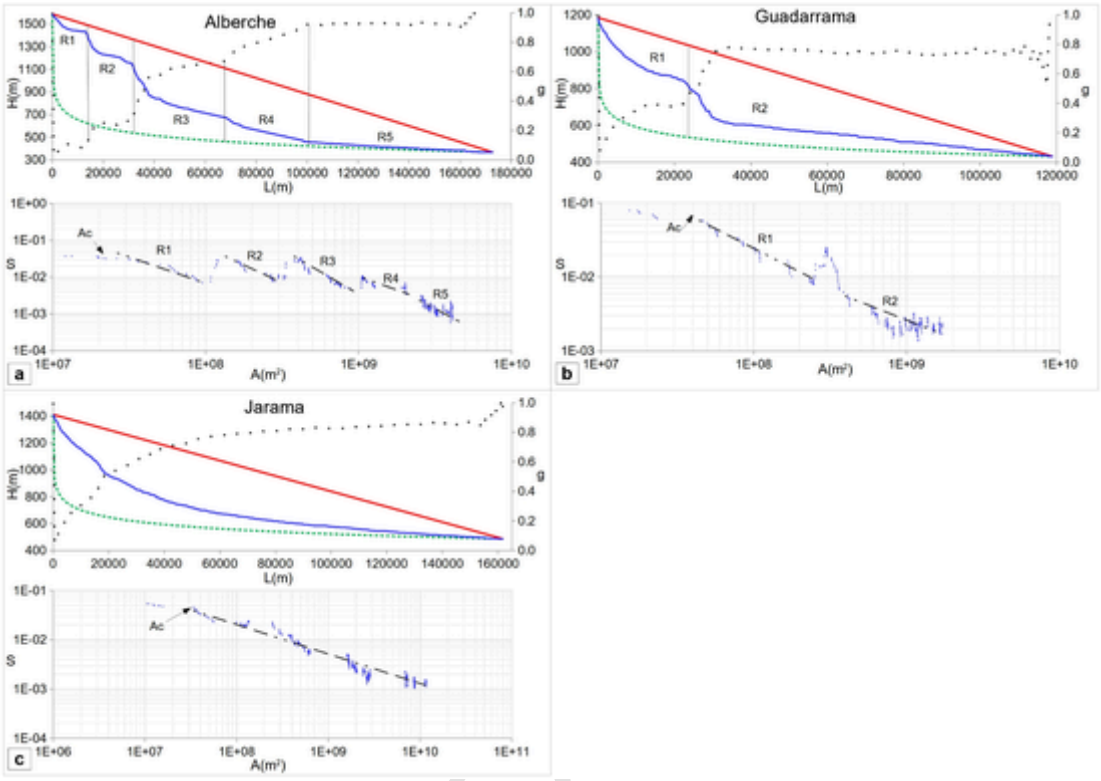

Fig. 6. Streams draining the southern flank reliefs of the Spanish Central System. The solid blue line represents the longitudinal profiles plotted together with the theoretical longitudinal profile (green dashed line) of each river. The g values are shown as a sequence of points. The straight red line is the reference with respect to which the indices have been calculated. The different identified reaches are shown for each long profile, along with the corresponding slope-area plots (log *S* vs. log *A*). *Ac* marks the transition to fluvial scaling. These three longitudinal profiles are clearly different from each other, without common morphometric features beyond a marked difference between the closeness of the theoretical and real long profiles in the lower-middle section, and the distance between these profiles in the upper-middle section. See the text for a detailed interpretation. (For interpretation of the references to colour in this figure legend, the reader is referred to the web version of this article.)

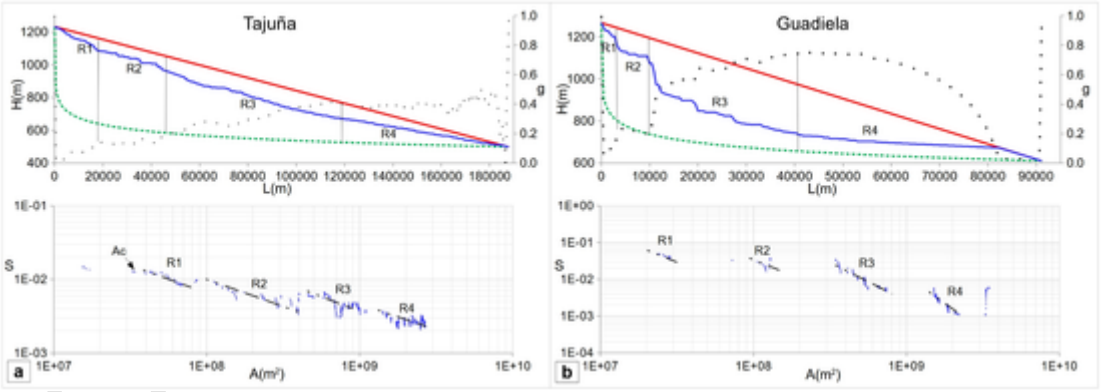

Fig. 7. Streams draining the western flank reliefs of the Iberian Range. The solid blue line represents the longitudinal profiles plotted together with the theoretical longitudinal profile (green dashed line) of each river. The g values are shown as a sequence of points. The straight red line is the reference with respect to which the indices have been calculated. The different identified reaches are shown for each long profile, along with the corresponding slope-area plots (log *S* vs. log *A*). *Ac* marks the transition to fluvial scaling. These are two longitudinal profiles of quite different geometries, although they share a similar g-value trend for the first three reaches. See the text for a detailed interpretation. (For interpretation of the references to colour in this figure legend, the reader is referred to the web version of this article.)

what attenuated due to the effect of downstream incision in the softer materials of the Duero Basin fill first and in the Catalayud Basin later (Fig. 3). The anomaly is found in the longitudinal profile of the Guadiela River. Although the g-value trend shows, as in the other cases, a downstream erosive deficit from R2 (Fig. 7), this trend is reversed in R4. Additionally, although the S-A plot records a typical slope-break-knickpoints pattern, the corresponding *Ksn* values do not rise downstream (Table 1). A possible explanation lies in the fact that this river does not completely outflank the Iberian Range and ends right in the mountainous front, coinciding with the Sierra de Altomira thrust front (Fig. 3). This thrust front leaves behind, to the east, the Loranca piggy-back basin, which became endorheic due to its disconnection from the Madrid Basin (Díaz-Molina and Tortosa, 1996) and in which the Guadiela River incises deep.

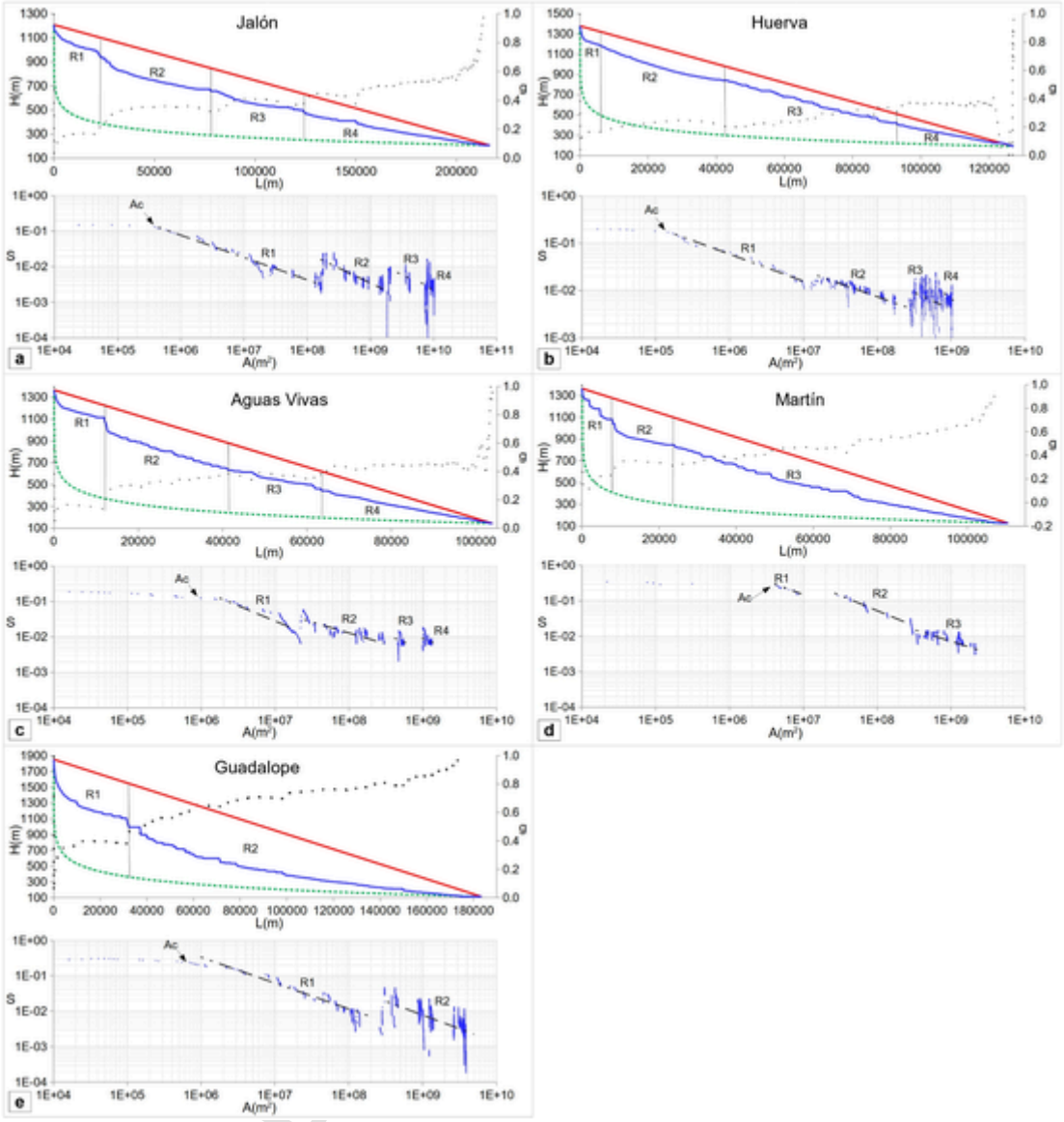

Fig. 8. Streams draining the eastern flank reliefs of the Iberian Range. The solid blue line represents the longitudinal profiles plotted together with the theoretical longitudinal profile (green dashed line) of each river. The g values are shown as a sequence of points. The straight red line is the reference with respect to which the indices have been calculated. The different identified reaches are shown for each long profile, along with the corresponding slope-area plots (log *S* vs. log *A*). *Ac* marks the transition to fluvial scaling. The elevation coincidence of the end of R1 stands out. It is clear that the longitudinal profiles have a low concavity geometry; they also have a constant proportional distance to the theoretical long profile. See the text for a detailed interpretation. (For interpretation of the references to colour in this figure legend, the reader is referred to the web version of this article.)

The results also show a coincidence in the inflection-point elevation of the g-value sequence in the longitudinal profiles of the rivers that drain the northern flank of the Spanish Central System. It occurs around elevations from 1050 to 1100 m asl (Fig. 5). The reach upstream of this inflection, R1, presents a sequence of increasing g values, and R2 presents a sequence of constant, very high values. It also roughly coincides with the path the rivers follow through the mountain front. There is a lithological contrast between the sedimentary fills of the basin and the rocky outcrops of the mountain range (Fig. 3). Thus, the rivers incise towards softer materials but develop a constant gradient, so there is no erosional deficit. They are very regularized rivers that only diverge in the headwaters. The Adaja River is somewhat of an anomaly in this case, first of all, because the change in the g-value trend coincides with a great knickpoint. The corresponding sequence with R1 begins to decrease slightly almost immediately (Fig. 5). The aforementioned knickpoint also coincides with a change in the horizontal direction of the river, in addition to its path through the mountainous front (Fig. 3). R1 incises into a small Cenozoic internal basin called Campoazálvaro (De Vicente et al., 2011) (Fig. 3). Thus, the record of g can be interpreted by considering an elbow capture by a creek (Tortosa et al., 1997; Gutiérrez-Elorza et al., 2005; Antón et al., 2014). The erosive excess that is recorded in the g values in R1 indicates that previously the long profile was regularized to a different outlet, which experiences a sharp drop in elevation. A third reach, R3, is differentiated based on the g values (Fig. 5). The change from R2 to R3 does not correspond to an inflection in the long profile. The g-value sequence changes from being constant to having a rising trend. This indicates an erosive deficit of R3 with respect to R2, coinciding with the union of a tributary. Hence, this suggests a competition to be the main stem, as a result of an autogenic river-basin reorganization (Scheingross et al., 2020). The decreasing sequences in the S-A plot, together with the decreasing *Ksn* values downstream, corroborate the influence of the lithological contrast in the

headwaters. In the case of the Adaja River, the increase of S in the S-A plot that separates R1 and R2 does not coincide with an increase in the *Ksn* value, which supports the interpretation of the capture. The transition between R2 and R3 coincides with a significant increase in area, which explains the effects of the union of a large tributary.

In contrast, the southern flank has a different pattern. Although it also contains rivers with a high regularization level, the values of g show an adaptation of each river to its particular geological context. The staggered sequence of g identifies reaches R1 and R2 of the Alberche River as two chained longitudinal profiles (Fig. 6). The integration of the Alberche River has been described as an upstream capture sequence (Díez Herrero, 2003). The ascending sequences of g values associated with R3 and R4 (Fig. 6) imply a successive erosive deficit, coinciding with the flow through the mountain front and the thrust of the southern edge, where the river abruptly changes direction (Fig. 3). Next, in R5, the g values indicate a high level of regularization. We can first infer that the river incises more easily into the filling materials of the Upper Tagus Basin, in the preferential thrust direction. However, the lithological contrast upstream is not large enough to explain why R3 and R4 show such an erosional deficit. The literature has traditionally described this area as one of low tectonic activity (e.g., Tejero et al., 2006; Galve et al., 2020). Nevertheless, the southern edge thrust is an active structure whose intensity decreases towards the north-east (Sanz de Galdeano et al., 2020). We found, in the long profile of the Alberche River, a signal suggesting differential uplift, which explains the erosional deficit of R3 and R4 with respect to the previous and subsequent reaches. The g values make it possible to identify a marked vertical-step knickpoint that divides the longitudinal profile of the Guadarrama River into two reaches (Fig. 6). It coincides with a lithological contrast (Fig. 3), and we could consider it an anchored knickpoint since, downstream, the river incises in a low-erodibility reach (Whipple et al., 2013). In the longitudinal profile of the Jarama River, the increasing trend, attenuated downstream, of g values indicates an erosive deficit upstream. This river crosses a lithological contrast, similar to the Guadarrama River, which explains the lower level of regularization of its upper-middle section. The Alberche River record in the S-A plot is typical of a sequence of slope-break knickpoints (Fig. 6), and the *Ksn* values increase downstream to R3 (Table 1), which supports the idea of a certain increase in the uplift ratio. The fact that the values decrease in R4 and R5 corroborates the high level of incision through the preferential thrust direction. The Guadarrama River presents a typical vertical-step knickpoint record in the S-A plot (Whipple et al., 2013), with similar *Ksn* values for the corresponding reaches. In the case of the Jarama River, we did not find a particular record in the S-A plot and *Ksn* values (Fig. 6 and Table 1).

6. Conclusions

The regularization level of a river in terms of dynamic equilibrium normally implies a smooth concave shape of its longitudinal profile. However, different resistance substrates require different equilibrium slopes, although they may have constant gradients. The shape that corresponds to a constant gradient can be reconstructed by a mathematical procedure. This provides a reference against which the shape of a real long profile can be quantified. The value, and its variations, of the differences between real and theoretical long profiles is a valuable record of the forcings that condition fluvial evolution. The approach presented in this work makes it possible to quantify the global regularization level of a river by calculating the stream regularization index (G). Quantitative comparisons can be established between different rivers within the same basin or in different basins, and provides a reference value to infer the maturity level of a river with respect to a certain conditions. On the other hand, this methodology also makes it possible to identify regime transitions through the calculation of regularization index (g) at discrete distances along the long profile. These transitions are recorded in changes in the g-value trend. When the changes correspond to knickpoints, their typology can also be established; this, along with the context, offers the possibility of identifying tectonic bounds. The calculation of g also makes it possible to discriminate between knickpoints and knicknoise when calculations are being performed on a large scale. The usefulness of the proposed indices has been verified by studying the selected examples, which represent different well-known tectonic contexts. Results are consistent with differences in the uplift ratio between the Iberian Range and the Spanish Central System and between distinct areas of the Spanish Central System, and highlights the influence of the structural asymmetry of the Spanish Central System on the incision patterns of the rivers. In general, it can be verified that the rivers draining into the Duero Basin have a high regularization level that is associated with a relict base level. The rivers draining into the Upper Tagus Basin have a medium regularization level, with differential uplift records that are highly influenced by the lithology, so that the signals are somewhat attenuated. The rivers that flow into the Ebro Basin present a low regularization level but clearly register signals of different uplift ratios between the range and basin, even where a long-term incision deceleration pattern has been documented. The results agree with the idea of a diachronic reorganization of the drainage networks, motivated by the opening of the respective basins, given the marked differences in the general and local regularization levels of the examples. These differences, in turn, are related to different settings. The comparison with the *S-A* plot and *Ksn* values has allowed us to corroborate the interpretations derived from the G and g indices regarding the identification of knickpoints and influential processes in the evolution of rivers. However, at the same time, we have been able to see that, especially for low-slope sections for which the data noise is more pronounced when a DEM is used for data extraction and large areas are covered, this method makes it easier to identify regime transitions, detect imperfections or knicknoise, and identify reaches with different channel steepness values.

Declaration of competing interest

The authors declare that they have no known competing financial interests or personal relationships that could have appeared to influence the work reported in this paper.

Data availability

Data will be made available on request.

Acknowledgements

This is work was supported by MARIBNO project, funded by the Spanish Ministry of Science, Innovation and Universities (Plan Estatal de Investigación Científica y Técnica y de Innovación; Ref. PGC2018-095999-B-100). We thank the editor Dr. Achim A. Beylich and two anonymous reviewers for their constructive reviews on the manuscript, which helped us to improve the initial version. We thank Dr. Ángel Soria-Jáuregui for comments and suggestions. UNED funding for open access publishing.

References

Antón, L., Rodés, A., De Vicente, G., Pallàs, R., Garcia-Castellanos, D., Stuart, F.M., Braucher, R., Bourlès, D., 2012. Quantification of fluvial incision in the Duero Basin (NW Iberia) from longitudinal profile analysis and terrestrial cosmogenic nuclide concentrations. Geomorphology 165–166, 50–61. https://doi.org/10.1016/j.geomorph.2011.12.036.

Antón, L., De Vicente, G., Muñoz-Martín, A., Stokes, M., 2014. Using river long profiles and geomorphic indices to evaluate the geomorphological signature of continental scale drainage capture, Duero Basin (NW Iberia). Geomorphology 206, 250–261. https://doi.org/10.1016/j.geomorph.2013.09.028.

Antón, L., Muñoz-Martín, A., De Vicente, G., 2019. Quantifying the erosional impact of a continental-scale drainage capture in the Duero Basin, Northwest Iberia. Quat. Res.

91 (2), 457–471. https://doi.org/10.1017/qua.2018.38.
Benito-Calvo, A., Moreno, D., Fujioka, T., López, G.I., Martín-González, F., Martínez-Fernández, A., Hernando-Alonso, I., Karampaglidis, T., Bermúdez de Castro, J.M., Gutiérrez, F., 2022. Towards the steady state? A long-term river incision deceleration pattern during Pleistocene entrenchment (Upper Ebro River, Northern Spain). Glob. Planet. Chang. 213, 103813. https://doi.org/10.1016/j.gloplacha.2022.103813.
Bishop, P., 2007. Long-term landscape evolution: linking tectonics and surface processes. Earth Surf. Process. Landf. 32, 329–365. https://doi.org/10.1002/esp.1493.
Boulton, S.J., Stokes, M., 2018. Which DEM is best for analyzing fluvial landscape development in mountainous terrains? Geomorphology 310, 168–187. https://doi.org/10.1016/j.geomorph.2018.03.002.
Bridgland, D.R., Westaway, R., Hu, Z., 2020. Basin inversion: a worldwide Late Cenozoic phenomenon. Glob. Planet. Chang. 193, 103260. https://doi.org/10.1016/j.gloplacha.2020.103260.
Caride de Liñán, C., 1994. Mapa Geológico de la Península Ibérica, Baleares y Canarias. Escala 1:1.000.000 (bajo la dirección de). Instituto Tecnológico Geominero de España.
Chauveau, D., Authemayou, C., Molliex, S., Godard, V., Benedetti, L., Pedoja, K., Husson, L., Yudawati Cahyarini, S., ASTER Team, 2021. Eustatic knickpoint dynamics in an uplifting sequence of coral reef terraces, Sumba Island, Indonesia. Geomorphology 393, 107936. https://doi.org/10.1016/j.geomorph.2021.107936.
Chilton, K.D., Spotila, J.A., 2022. Uncovering the controls on fluvial bedrock erodibility and knickpoint expression: a high-resolution comparison of bedrock properties between knickpoints and non-knickpoint reaches. J.Geophys.Res.Earth Surf. 127 (3), e2021JF006511. https://doi.org/10.1029/2021JF006511.
Clubb, F.J., Mudd, S.M., Attal, M., Milodowski, D.T., Grieve, S.W., 2016. The relationship between drainage density, erosion rate, and hilltop curvature: Implications for sediment transport processes. J.Geophys.Res.Earth Surf. 121 (10), 1724–1745. https://doi.org/10.1002/2015JF003747.
Conway-Jones, B.W., Roberts, G.G., Fichtner, A., Hoggard, M., 2019. Neogene epeirogeny of Iberia. Geochem. Geophys. Geosyst. 20, 138–1163. https://doi.org/10.1029/2018GC007899.
Cunha, P.P., Martins, A.A., Gomes, A., Stokes, M., Cabral, J., Lopes, F.C., Pereira, D., de Vicente, G., Buylaert, J.-P., Murray, A.S., Antón, L., 2019. Mechanisms and age estimates of continental-scale endorheic to exorheic drainage transition: Douro River, Western Iberia. Glob. Planet. Chang. 181, 102985. https://doi.org/10.1016/j.gloplacha.2019.102985.
Davis, W.M., 1902. Baselevel, grade and peneplain. J. Geol. 10, 77–111.
De Vicente, G., Vegas, R., Muñoz Martín, A., Silva, P.G., Andriessen, P., Cloetingh, S., González Casado, J.M., Van Wees, J.D., Álvarez, J., Carbó, A., Olaiz, A., 2007. Cenozoic thick-skinned deformation and topography evolution of the Spanish Central System. Glob. Planet. Chang. 58, 335–381. https://doi.org/10.1016/j.gloplacha.2006.11.042.
De Vicente, G., Cloetingh, S.A.P.L., VanWees, J.D., Cunha, P.P., 2011. Tectonic classification of Cenozoic Iberian foreland basins. Tectonophysics 502, 38–61. https://doi.org/10.1016/j.tecto.2011.02.007.
De Vicente, G., Cunha, P.P., Muñoz-Martín, A., Cloetingh, S.A.P.L., Olaiz, A., Vegas, R., 2018. The Spanish-Portuguese Central System: an example of intense intraplate deformation and strain partitioning. Tectonics 37 (12), 4444–4469. https://doi.org/10.1029/2018TC005204.
Demoulin, A., 1998. Testing the tectonic significance of some parameters of longitudinal river profiles: the case of the Ardenne (Belgium, NW Europe). Geomorphology 24, 189–208. https://doi.org/10.1016/S0169-555X(98)00016-6.
Demoulin, A., Mather, A., Whittaker, A., 2016. Fluvial archives, a valuable record of vertical crustal deformation. Quat. Sci. Rev. 166, 10–37. https://doi.org/10.1016/j.quascirev.2016.11.011.
Díaz-Molina, M., Tortosa, A., 1996. Fluvial fans of the Loranca Basin, Late Oligocene-Early Miocene. In: Friend, P.F., Dabrio, C.J. (Eds.), Tertiary Basins of Spain: The Stratigraphic Record of Crustal Kinematics. Cambridge University Press, Cambridge, p. 399.
Díez Herrero, A., 2003. Geomorfología e hidrología fluvial del río Alberche: modelos y S.I.G. para la gestión de riberas. Ph.D. Thesis. Universidad Complutense de Madrid, Madrid, Spain. (610 pp.).
Eckert, S., Kellenberger, T., Itten, K., 2005. Accuracy assessment of automatically derived digital elevation models from aster data in mountainous terrain. Int. J. Remote Sens. 26 (9), 1943–1957. https://doi.org/10.1080/01431160420002983O6.
England, P., Molnar, P., 1990. Surface uplift, uplift of rocks, and exhumation of rocks. Geology 18, 1173–1177. https://doi.org/10.1130/0091-7613(1990)018.
Flint, J.J., 1974. Stream gradient as a function of order, magnitude, and discharge. Water Resour. Res. 10, 969–973. https://doi.org/10.1029/WR010i005p00969.
Gailleton, B., Mudd, S.M., Clubb, F.J., Peifer, D., Hurst, M.D., 2019. A segmentation approach for the reproducible extraction and quantification of knickpoints from river long profiles. Earth Surf. Dynam. 7, 211–230. https://doi.org/10.5194/esurf-7-211-2019.
Galve, J.P., Pérez-Peña, J.V., Azañón, J.M., Insua Pereira, D.M., Cunha, P.P., Pereira, P., Ortuño, M., Viaplana-Muzas, M., Gracia Prieto, F.J., Remondo, J., Jabaloy, A., Bardají, T., Silva, P.G., Lario, J., Zazo, C., Goy, J.L., Dabrio, C.J., Cabero, A., 2020. Active landscapes of Iberia. In: Quesada, C., Oliveira, J. (Eds.), The Geology of Iberia: A Geodynamic Approach. Regional Geology Reviews. Springer, Cham, pp. 77–124. https://doi.org/10.1007/978-3-030-10931-8_5.
Garcia-Castellanos, D., Larrasoaña, J.C., 2015. Quantifying the post–tectonic topographic evolution of closed basins: the Ebro Basin (northeast Iberia). Geology 43, 663–666. https://doi.org/10.1130/G36673.1.
García-Mayordomo, J., Insua-Arévalo, J.M., Martínez-Díaz, J.J., Jiménez-Díaz, A., Martín-Banda, R., Martín-Alfageme, S., Álvarez-Gómez, J.A., Rodríguez-Peces, M., Pérez-López, R., Rodríguez-Pascua, M.A., Masana, E., Perea, H., Martín-González, F., Giner-Robles, J., Nemser, E.S., Cabral, J., Sanz de Galdeano, C., Peláez, J.A., García-Tortosa, F., Grácia, E., Bartolomé, R., González, Á., Azañón, J.M., Alfaro, P., Moreno, X., Ferrero-Vega, A., Dias, R., Martínez, S., Gutiérrez, F., Ortuño, M., Booth-Rea, G., Giaconia, F., Martínez-Martínez, J.M., Villegas, I., Lo Lacono, C., Pérez-Peña, V., Martín-González, F., Brum de Silveira, A., García-Meléndez, E., Lafuente, P., Simón, J.L., Arlegui, L.E., Liesa, C.L., Bach, J., Linares, R., 2012. The Quaternary active faults database of Iberia (QAFI v. 2.0). J. Iber. Geol. 38 (1), 285–302. https://doi.org/10.5209/rev_JIGE.2012.v38.n1.39219.
Gasparini, N.M., Bras, R.L., Whipple, K.X., 2006. Numerical modeling of non-steady-state river profile evolution using a sediment-flux-dependent incision model. Spec. Pap. Geol. Soc. Am. 398, 127–141.
Giachetta, E., Molin, P., Scotti, V.N., Faccenna, C., 2015. Plio-Quaternary uplift of the Iberian Chain (Central–Eastern Spain) from landscape evolution experiments and river profile modeling. Geomorphology 246, 48–67. https://doi.org/10.1016/j.geomorph.2015.06.005.
Gilbert, G.K., 1877. Geology of the Henry Mountains. U.S.G.S. Printing Office, Washington, D.C. https://doi.org/10.3133/70038096.
Goldrick, G., Bishop, P., 2007. Regional analysis of bedrock stream long profiles: Evaluation of Hack's SL form, and formulation and assessment of an alternative (the DS form). Earth Surf. Process. Landf. 32, 649–671. https://doi.org/10.1002/esp.1413.
Gonga-Saholiariliva, N., Gunnell, Y., Harbor, D., Mering, C., 2011. An automated method for producing synoptic regional maps of river gradient variation: procedure, accuracy tests, and comparison with other knickpoint mapping methods. Geomorphology 134 (3–4), 394–407. https://doi.org/10.1016/j.geomorph.2011.07.013.
Goren, L., Fox, M., Willett, S.D., 2014. Tectonics from fluvial topography using formal linear inversion: Theory and applications to the Inyo Mountains,California. J. Geophys. Res. Earth Surf. 119, 1651–1681. https://doi.org/10.1002/2014JF003079.
Guimerá, J., 2018. Structure of an intraplate fold-and-thrust belt: the Iberian Chain.A synthesis. Geol. Acta 16 (4), 427–438. https://doi.org/10.1344/GeologicaActa2018.16.4.6.
Guimerá, 2022. Large-scale structure of an Intraplate Fold-and-Thrust Belt: the Iberian Chain. Geo-Temas 18, 76–78. . http://hdl.handle.net/2445/184786.
Guimerá, J., Mas, R., Alonso, Á., 2004. Intraplate deformation in the NW Iberian Chain: Mesozoic extension and Tertiary contractional inversion. J. Geol. Soc. 161 (2), 291–303. https://doi.org/10.1144/0016-764903-055.
Gutiérrez-Elorza, M., Desir, G., Gutiérrez-Santolalla, F., Marín, C., 2005. Origin and evolution of playas and blowouts in the semiarid zone of Tierra de Pinares (Duero Basin, Spain). Geomorphology 72 (1–4), 177–192. https://doi.org/10.1016/j.geomorph.2005.05.009.
Hack, J., 1957. Studies of longitudinal stream profiles in Virginia and Maryland. In: US Geol. Surv. Profess. Paper 294-B. pp. 45–97.
Hack, J., 1973. Stream-profiles analysis and stream-gradient index. J. Res. US Geol. Surv. 1, 421–429.
Hack, J., 1975. Dynamic equilibrium and landscape evolution. In: Melhorn, W.N., Flemal, R.C. (Eds.), Theories of Landform Development. State Univ. of New York, New York, pp. 87–102.
Harel, M.A., Mudd, S., Attal, M., 2016. Global analysis of the stream power law parameters based on worldwide 10Be denudation rates. Geomorphology 268, 184–196. https://doi.org/10.1016/j.geomorph.2016.05.035.
Haviv, I., Enzel, Y., Whipple, K.X., Zilberman, E., Matmon, A., Stone, J., Fifield, K.L., 2010. Evolution of vertical knickpoints (waterfalls) with resistant caprock: Insights from numerical modeling. J.Geophys.Res.Earth Surf. 115, F03028. https://doi.org/10.1029/2008JF001187.
Hayakawa, Y., Oguchi, T., 2006. DEM-based identification of fluvial knickzones and its application to Japanese mountain rivers. Geomorphology 78, 90–106. https://doi.org/10.1016/j.geomorph.2006.01.018.
Hergarten, S., 2020. Rivers as linear elements in landform evolution models. Earth Surf. Dynam. 8, 367–377. https://doi.org/10.5194/esurf-8-367-2020.
Hovius, N., 2000. Macroscale process systems of mountain belt erosion. In: Summerfield, M.A. (Ed.), Geomorphology and global tectonics. Wiley & Sons, Chichester, pp. 77–105.
Howard, A.D., Dietrich, W., Seidl, M., 1994. Modeling fluvial erosion on regional to continental scale. J. Geophys. Res. 99B, 13971–13986. https://doi.org/10.1029/94JB00744.
Jarvis, A., Reuter, H.I., Nelson, A., Guevara, E., 2008. Hole-filled seamless SRTM data V4. International Centre for Tropical Agriculture (CIAT). http://srtm.csi.cgiar.org.
Karampaglidis, T., Benito-Calvo, A., Rodés, A., Braucher, R., Pérez-González, A., Pares, J., Stuart, F., Di Nicola, L., Bourles, D., 2020. Pliocene endorheic-exoreic drainage transition of the Cenozoic Madrid Basin (Central Spain). Glob. Planet. Chang. 194, 103295. https://doi.org/10.1016/j.gloplacha.2020.103295.
Kirby, E., Whipple, K.X., 2012. Expression of active tectonics in erosional landscapes. J. Struct. Geol. 44, 54–75. https://doi.org/10.1016/j.jsg.2012.07.009.
Kwang, J.S., Parker, G., 2017. Landscape evolution models using the stream power incision model show unrealistic behavior when m n equals 0.5. Earth Surf.Dyn. 5, 807–820. https://doi.org/10.5194/esurf-5-807-2017.
Lague, D., 2014. The stream power river incision model: evidence, theory and beyond. Earth Surf. Process. Landf. 39, 38–61. https://doi.org/10.1002/esp.3462.
Mackin, J., 1948. Concept of the graded river. Bull. Geol. Soc. Am. 59, 463–512.
Martín-Serrano, A., 1991. La definición y el encajamiento de la red fluvial actual sobre el macizo Hespérico en el marco de su geodinámica alpina. Rev. Soc. Geol. Esp. 4, 337–351.
Montgomery, D.R., Foufoula-Georgiou, E., 1993. Channel network source representation using digital elevation models. Water Resour. Res. 29, 3925–3934. https://doi.org/10.1029/93WR02463.
Morisawa, M.E., 1962. Quantitative geomorphology of some watersheds in the

Appalachian Plateau. Geol. Soc. Am. Bull. 73, 1025. https://doi.org/10.1130/0016-7606(1962)73[1025:QGOSWI]2.0.CO;2.
Morris, P., Williams, D., 1997. Exponential longitudinal profiles of streams. Earth Surf. Process. Landf. 22, 143–163. https://doi.org/10.1002/(SICI)1096-9837(199702)22:2%3C143::AID-ESP681%3E3.0.CO;2-Z.
Mudd, S.M., Clubb, F.J., Gailleton, B., Hurst, M.D., 2018. How concave are river channels? Earth Surf. Dyn. Discuss 6, 505–523. https://doi.org/10.5194/esurf-2018-7.
Neely, A.B., Bookhagen, B., Burbank, D.W., 2017. An automated knickzone selection algorithm (KZ-Picker) to analyze transient landscapes: calibration and validation. J. Geophys. Res. Earth Surf. 122, 1236–1261. https://doi.org/10.1002/2017JF004250.
Oliva, M., Palacios, D., Fernández-Fernández, J.M., Rodríguez-Rodríguez, L., García-Ruiz, J.M., Andrés, N., Carrasco, R.M., Pedraza, J., Pérez-Alberti, A., Valcarcel, M., Hughes, P.D., 2019. Late Quaternary glacial phases in the Iberian Peninsula. Earth Sci. Rev. 192, 564–600. https://doi.org/10.1016/j.earscirev.2019.03.015.
Pastor-Martín, C., Antón, L., Fernández-González, C., 2018. FLUNETS: a new MATLAB–based tool for drainage network ordering by Horton and Hack hierarchies. Geogr. Tech. 13, 114–124. https://doi.org/10.21163/GT_2018.132.09.
Pereira, D., Alves, M., Araújo, M., Cunha, P.P., 2000. Estratigrafia e interpretação paleogeográfica do Cenozóico continental do norte de Portugal. Ciênc. Terra 14, 73–82.
Pérez-Obiol, R., Jalut, G., Julià, R., Pèlachs, A., Iriarte, M.J., Otto, T., Hernández-Beloqui, B., 2011. Mid-Holocene vegetation and climatic history of the Iberian Peninsula. The Holocene 21 (1), 75–93. https://doi.org/10.1177/0959683610384161.
Pérez-Peña, J., Azañon, J., Azor, A., Delgado, J., Gonzalez-Lodeiro, F., 2009. Spatial analysis of stream power using GIS: SLk anomaly maps. Earth Surf. Process. Landf. 34, 16–25. https://doi.org/10.1002/esp.1684.
Perron, J.T., Royden, L., 2013. An integral approach to bedrock river profile analysis. Earth Surf. Process. Landf. 38, 570–576. https://doi.org/10.1002/esp.3302.
Piacentini, D., Francesco, T., Tommaso, S., Olivia, N., Francesco, V., 2020. SLiX: a GIS toolbox to support along-stream knickzones detection through the computation and mapping of the stream length-gradient (SL) index. ISPRS Int. J. Geo Inf. 9 (2), 69. https://doi.org/10.3390/ijgi9020069.
Queiroz, G.L., Salamuni, E., Nascimento, E.R., 2015. Knickpoint finder: a software tool that improves neotectonic analysis. Comput. Geosci. 76, 80–87. https://doi.org/10.1016/j.cageo.2014.11.004.
Rat, J., Mouthereau, F., Brichau, S., Crémades, A., Bernet, M., Balvay, M., Ganne, J., Lahfid, A., Gautheron, C., 2019. Tectonothermal evolution of the Cameros Basin: implications for tectonics of North Iberia. Tectonics 38, 440–469. https://doi.org/10.1029/2018TC005294.
Regard, V., Vacherat, A., Bonnet, S., Mouthereau, F., Nørgaard, J., Knudsen, M.F., 2021. Late Pliocene-Pleistocene incision in the Ebro Basin (North Spain). BSGFEarth Sci.Bull. 192 (1), 30. https://doi.org/10.1051/bsgf/2021020.
Rice, S., Church, M., 2001. Longitudinal profiles in simple alluvial systems. Water Resour. Res. 37, 417–426. https://doi.org/10.1029/2000WR900266.
Rodrigo-Comino, J., Senciales González, J.M., 2015. Ratio LE para el ajuste de perfiles longitudinales en cursos fluviales de montaña. Aplicación a la cuenca del río Almáchar (Málaga, España). Cuaternario Geomorfol. 29 (3–4), 57–76.
Rodríguez-Rodríguez, L., Antón, L., Rodés, Á., Pallàs, R., García-Castellanos, D., Jiménez-Munt, I., Struth, L., Leanni, L., 2020. Dates and rates of endo-exorheic drainage development: insights from fluvial terraces (Duero River, Iberian Peninsula). Glob. Planet. Chang. 193, 103271. https://doi.org/10.1016/j.gloplacha.2020.103271.
Roe, G.H., Montgomery, D.R., Hallet, B., 2002. Effects of orographic precipitation variations on the concavity of steady-state river profiles. Geology 30, 143. https://doi.org/10.1130/0091-7613(2002)030<0143:EOOPVO>2.0.CO;2.
Santisteban, J.I., Schulte, L., 2007. Fluvial networks of the Iberian Peninsula; a chronological framework. Quat. Sci. Rev. 26, 2738–2757. https://doi.org/10.1016/j.quascirev.2006.12.019.
Santisteban, J.I., Mediavilla, R., Martín-Serrano, A., Dabrio, C.J., 1996. The Duero Basin: a general overview. In: Friend, P.F., Dabrio, C.J. (Eds.), Tertiary Basins of Spain: The Stratigraphic Record of Crustal Kinematics. Cambridge Univ. Press, Cambridge, UK, pp. 183–187.
Sanz de Galdeano, C., Azañón, J.M., Cabral, J., Ruano, P., Alfaro, P., Canora, C., Ferrater, M., García Tortosa, F.J., García-Mayordomo, J., Gràcia, E., Insua-Arévalo, J.M., Jiménez Bonilla, A., Lacan, P.G., Marín-Lechado, C., Martín-Banda, R., Martín González, F., Martínez-Díaz, J.J., Martín-Rojas, I., Masana, E., Ortuño, M., Pedrera, A., Perea, H., Simón, J.L., 2020. Active faults in Iberia. In: Quesada, C., Oliveira, J. (Eds.), The Geology of Iberia: A Geodynamic Approach. Regional Geology Reviews. Springer, Cham, pp. 33–75. https://doi.org/10.1007/978-3-030-10931-8_4.
Sassolas-Serrayet, T., Cattin, R., Ferry, M., Godard, V., Simoes, M., 2019. Estimating the disequilibrium in denudation rates due to divide migration at the scale of river basins. Earth Surf. Dyn. 7, 1041–1057. https://doi.org/10.5194/esurf-7-1041-2019.
Scheingross, J.S., Limaye, A.B., McCoy, S.W., Whittaker, A.C., 2020. The shaping of erosional landscapes by internal dynamics. Nat. Rev. Earth Environ. 1 (12), 661–676. https://doi.org/10.1038/s43017-020-0096-0.
Schwanghart, W., Scherler, D., 2014. TopoToolbox 2–MATLAB-based software for topographic analysis and modeling in Earth surface sciences. Earth Surface Dyn. 2 (1), 1–7. https://doi.org/10.5194/esurf-2-1-2014.
Shaler, N.S., 1899. Spacing of rivers with reference to hypothesis of baseleveling. Geol. Soc. Am. Bull. 10, 263–276. https://doi.org/10.1130/GSAB.
Sklar, L., Dietrich, W.E., 1998. River longitudinal profiles and bedrock incision models: stream power and the influence of sediment supply. In: Tinkler, J., Wohl, E. (Eds.), Geophysical Monograph Series. American Geophysical Union, Washington, D.C., pp. 237–260. https://doi.org/10.1029/GM107p0237.
Snow, R., Slingerland, R., 1987. Mathematical modeling of graded river profiles. J. Geol. 95, 15–33. https://doi.org/10.1086/629104.
Soria-Jáuregui, Á., Jiménez-Cantizano, F., Antón, L., 2019. Geomorphic and tectonic implications of the endorheic to exorheic transition of the Ebro River system in Northeast Iberia. Quat. Res. 91, 472–492. https://doi.org/10.1017/qua.2018.87.
Struth, L., Garcia-Castellanos, D., Viaplana-Muzas, M., Vergés, J., 2019. Drainage network dynamics and knickpoint evolution in the Ebro and Duero basins: from endorheism to exorheism. Geomorphology 327, 554–571. https://doi.org/10.1016/j.geomorph.2018.11.033.
Subiela Blanco, G.B., Guinau i Sellés, M., Galve Arnedo, J.P., 2019. Idoneidad del índice SL para la identificación semi-automática de movimientos en masa que afectan a la red de drenaje. Bol. Geol. Min. 130 (3), 465–487. https://doi.org/10.21701/bolgeomin.130.3.005.
Tarboton, D., Bras, R., Rodriguez-Iturbe, I., 1989. Scaling and elevation in river networks. Water Resour. Res. 25 (9), 2037–2051. https://doi.org/10.1029/WR025i009p02037.
Tejero, R., González-Casado, J.M., Gómez-Ortiz, D., Sánchez-Serrano, F., 2006. Insights into the "tectonic topography" of the present-day landscape of the central Iberian Peninsula (Spain). Geomorphology 76 (3–4), 280–294. https://doi.org/10.1016/j.geomorph.2005.11.007.
Tortosa, A., Arribas Mocoroa, J., Garzón Heydt, G., Fernández García, P., Palomares Herranz, M., 1997. Análisis petrológico de depósitos de terrazas aplicado al estudio de los procesos de captura en los ríos Adaja, Voltoya y Eresma (provincias de Segovia y Valladolid). Rev. Soc. Geol. España 10 (1–2), 131–145.
Troiani, F., Galve, J.P., Piacentini, D., Della Seta, M., Guerrero, J., 2014. Spatial analysis of stream length-gradient (SL) index for detecting hillslope processes: a case of the Gállego River headwaters (Central Pyrenees, Spain). Geomorphology 214, 183–197. https://doi.org/10.1016/j.geomorph.2014.02.004.
Vágó, J., 2010. Stream gradient investigation in the Bükkalja using interpolated surfaces. Landsc.Environ. 4 (1), 23–36. https://ojs.lib.unideb.hu/landsenv/article/view/2272. https://ojs.lib.unideb.hu/landsenv/article/view/2272.
Varrani, A., Nones, M., Gupana, R., 2019. Long-term modelling of fluvial systems at the watershed scale: examples from three case studies. J. Hydrol. 574, 1042–1052. https://doi.org/10.1016/j.jhydrol.2019.05.012.
Viveen, W., Baby, P., Hurtado-Enríquez, C., 2021. Assessing the accuracy of combined DEM-based lineament mapping and the normalised SL-index as a tool for active fault mapping. Tectonophysics 813, 228942. https://doi.org/10.1016/j.tecto.2021.228942.
Whipple, K.X., 2004. Bedrock rivers and the geomorphology of active orogens. Annu. Rev. Earth Planet. Sci. 32, 151–185. https://doi.org/10.1146/annurev.earth.32.101802.120356.
Whipple, K.X., Tucker, G.E., 1999. Dynamics of the stream-power river incision model: Implications for height limits of mountain ranges, landscape response timescales, and research needs. J. Geophys. Res. Solid Earth 104, 17661–17674. https://doi.org/10.1029/1999JB900120.
Whipple, K.X., Tucker, G., 2002. Implications of sediment-flux-dependent river incision models for landscape evolution. J. Geophys. Res. 107, 2039. https://doi.org/10.1029/2000JB000044.
Whipple, K.X., DiBiase, R.A., Crosby, B.T., 2013. Bedrock rivers. In: Shroder, J., Wohl, E. (Eds.), Treatise on Geomorphology. Fluvial Geomorphology, vol. 9. Academic Press, San Diego, CA, pp. 550–573. https://doi.org/10.1016/B978-0-12-374739-6.00254-2.
Whittaker, A., Boulton, S., 2012. Tectonic and climatic controls on knickpoint retreat rates and landscape response times. J. Geophys. Res. 117F, F02024. https://doi.org/10.1029/2011JF002157.
Whittaker, A., Cowie, P., Attal, M., Tucker, G., Roberts, G., 2007. Bedrock channel adjustment to tectonic forcing: implications for predicting river incision rates. Geology 35, 103–106. https://doi.org/10.1130/G23106A.1.
Wickert, A.D., Schildgen, T.F., 2019. Long-profile evolution of transport-limited gravel-bed rivers. Earth Surf. Dyn. 7, 17–43. https://doi.org/10.5194/esurf-7-17-2019.
Willett, S.D., Brandon, M.T., 2002. On steady states in mountain belts. Geology 30, 175–178. https://doi.org/10.1130/0091-7613(2002)030%3C0175:OSSIMB%3E2.0.CO;2.
Wobus, C., Whipple, K.X., Kirby, E., Snyder, N., Johnson, J., Spyropolou, K., Crosby, B., Sheehan, D., 2006. Tectonics from topography: procedures, promise, and pitfalls. In: Special Paper 398: Tectonics, Climate, And Landscape Evolution. Geological Society of America, pp. 55–74. https://doi.org/10.1130/2006.2398(04).
Zahra, T., Paudel, U., Hayakawa, Y.S., Oguchi, T., 2017. Knickzone extraction tool (KET) –a new ArcGIS toolset for automatic extraction of knickzones from a DEM based on multi-scale stream gradients. Open Geosci. 9 (1), 73–88. https://doi.org/10.1515/geo-2017-0006.